# Wind measurements and eddy-structure in the boundary layer using Volume-Imaging Lidar and Large-Eddy Simulation

Shane D. Mayor, Joseph P. Garcia, Gregory Tripoli, and Edwin W. Eloranta
Department of Atmospheric and Oceanic Sciences, University of Wisconsin
1225 W. Dayton St., Madison, Wisconsin, 53706, USA
phone: 608-263-7327, fax: 608-262-5974, e-mail: eloranta@lidar.ssec.wisc.edu

## 1. Introduction

Large-eddy simulations (LESs) provide an attractive way of developing parameterizations for global climate and weather forecast models. This is because they provide 4-D information with eddy-resolving resolution which can be used to compute fluxes with sampling errors that are much smaller than those made from in situ measurements. LESs, however, are only viable if we have confidence in their solutions. In particular, high-resolution 4-D measurements are needed to test the LESs ability to accurately simulate the organization of convection such as linear and cellular boundary layer circulations. The objective of our research is to demonstrate the usefulness of volume imaging lidar data in LES validation.

The University of Wisconsin's Volume-Imaging Lidar (UW-VIL) was deployed in Sheboygan, Wisconsin, for the Lake-Induced Convection Experiment (Lake-ICE) during the winter of 1997-98. The site was located within 10 m of the western shore of Lake Michigan to measure the 4-dimensional (space and time) structure of the internal boundary layer that forms over the relatively warm lake during westerly and northwesterly cold air outbreaks. The configuration of the VIL used in Lake-ICE allowed us to record backscatter intensity at 15-m intervals out to 18-km ranges.

The University-of-Wisconsin non-hydrostatic modeling system (UW-NMS) is our large-eddy simulation code. To simulate the internal boundary layer, we specify a domain that is 1.8-km wide in the north-south direction by 12-km in the east-west direction. The western 6-km of the domain is located over snow-covered land and eastern 6 km over 279 K water. A radiosonde sounding, taken 10-km west of the lidar site, is used to initialize the domain as horizontally homogeneous. A shear-driven mixed-layer develops over the land and advects over the water. The domain is periodic in both lateral directions. Vertical layers 900-m wide are installed in the east and west ends of the domain to restore the flow to its initial condition before re-entering the domain.

In previous work, algorithms were developed to measure vertical profiles of the horizontal wind from volumetric lidar images of aerosol structure [1, 2]. These algorithms derived a single wind vector for each altitude representing the mean wind averaged over the $\sim 100$- km$^2$ area of a typical lidar scan. In this paper, we extend these algorithms to allow computation of the spatial variation of winds from successive near-zero-degree-elevation azimuthal-scans.

## 2. Wind Measurements

Extracting wind vectors from the backscatter data follows the basic approach described by [2]. The only difference in the initial processing occurs because the scan consists of a single horizontal plane instead of a volume scan. The initial processing steps proceed as follows:

1. Individual lidar shots are corrected for the $r^{-2}$ dependence of the returned signal and then filtered with a running median high-pass filter. The filter length was set to 450 m for the results presented here.

2. The lidar data is mapped to a Cartesian grid with a uniform spatial resolution of 15 m. Data points on the Cartesian grid are computed from a linear interpolation between the 4 nearest points in the polar coordinates of the raw lidar-profiles. To correct for the distortion of the lidar image caused by the wind and a finite scan-duration, the position of data points in the lidar profiles are adjusted to the position they occupied at the time the first profile of the scan was acquired. The wind vector needed for this adjustment is estimated from a trial solution. The results of this solution are used for the distortion correction in the final wind solution.

3. A temporal-median image is then formed from the complete set of Cartesian scan-images. In order to remove stationary features and artifacts caused by attenuation, this median image is subtracted from each of the scan images.

4. Finally, to prevent individual bright features in the image from dominating the cross correlation

function, the resulting images are subjected to a histogram normalization.

Up to this point, the wind processing is nearly identical to the scheme for computing winds averaged over the entire scan area as described in Piironen and Eloranta. However, in order to compute the spatial variation of the wind field, the scan area must now be divided into smaller sub-areas. 2-D lag cross correlations are computed between successive scans in each of the sub-areas. These cross correlation-functions are then averaged over a series of scan pairs. Wind vectors are then computed from the lag positions of averaged correlation function maximums and the time separation between scans.

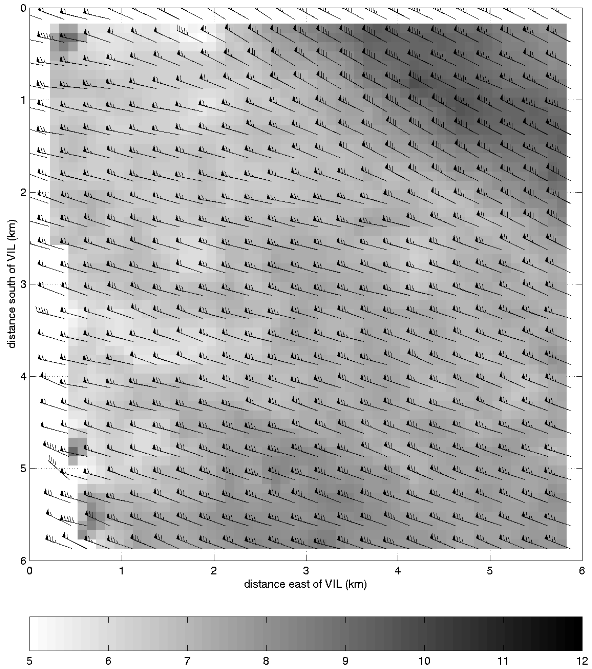

FIG. 1. Wind vectors computed from 40 PPI scans acquired between 10:24:44 and 10:32:17 CST on January 13, 1998. The background shading is proportional to wind speed in m/s. Meteorological wind barbs are presented with triangles indicating 5 m/s and single barbs indicating 1 m/s.

In the computations presented here, winds are calculated in square sub-areas which are 250 meters on a side. Correlations are computed between every other scan so that left-right/right-left scans are always paired with the same scan direction and thus the time interval between laser profiles in each part of successive images is approximately the same. This results in a ~ 24-s time separation between scans. Because the winds were as large as 9 m/s, the wind advected structures by up to 216 m between scans. This causes a problem with the cross correlation calculation because most of the structure seen in a sub-area in one scan has advected out of the sub-area by the time of the next scan. This creates small correlation maxima contaminated by random correlations between unrelated structures.

To minimize this problem, the correlation calculation is modified. The location of the sub-area in the second frame of each pair is displaced downwind by the distance the structure is expected to move between frames. This allows the correlation to take place with approximately the same features that were present in the first frame. The position of the correlation maximum is then corrected for the displacement of the box to compute the wind vector. An estimate of the wind vector is required in order to select the displacement for the sub-area in the second frame. This is computed by first generating a lower resolution wind field where the advection distance is a smaller fraction of the sub-area's size. For the winds shown below, the wind field was first calculated in square sub-areas with sides of 500 m. The 500-m values were then used to compute displacements for the four 250-m areas in each of the larger areas.

Fig. 1 shows the lidar-derived wind field observed on a horizontal plane 5 m above Lake Michigan's surface on January 13, 1998. The lidar was located within 10 m of the shoreline which is aligned roughly north-south. A slightly curving shoreline places the beach ~ 500 m west of the lidar at 3 km south of the lidar. It then curves to the east; placing the shore directly south of the lidar ~ 3.5 km south of the lidar. The shore reaches a maximum distance east of the lidar, ~ 350 m at ~ 6 km south of the lidar.

In fig. 1 a wind-speed maximum exists in the upper-right corner of the image. Because the wind is from the NW and the shape of the coastline, the air in this corner has a much larger fetch than the air from anywhere else in the image. Thus we conclude it is moving faster because it has had a longer time to accelerate than other points in the image.

The divergence and vorticity of the wind field can be computed from

$$\nabla \cdot \vec{V}_{i,j} = \frac{u_{i+1,j} - u_{i-1,j}}{x_{i+1} - x_{i-1}} + \frac{v_{i,j+1} - v_{i,j-1}}{y_{j+1} - y_{j-1}}$$

and

$$\nabla \times \vec{V}_{i,j} = \frac{v_{i+1,j} - v_{i-1,j}}{x_{i+1} - x_{i-1}} - \frac{u_{i,j+1} - u_{i,j-1}}{y_{j+1} - y_{j-1}},$$

respectively. These fields are shown in figs. 2 and 3. A band of convergence and negative vorticity appear in the region of the wind-speed gradient in the

NW corner of the image. Other bands elsewhere in the divergence field indicate the presence of lineal boundary layer roll structures.

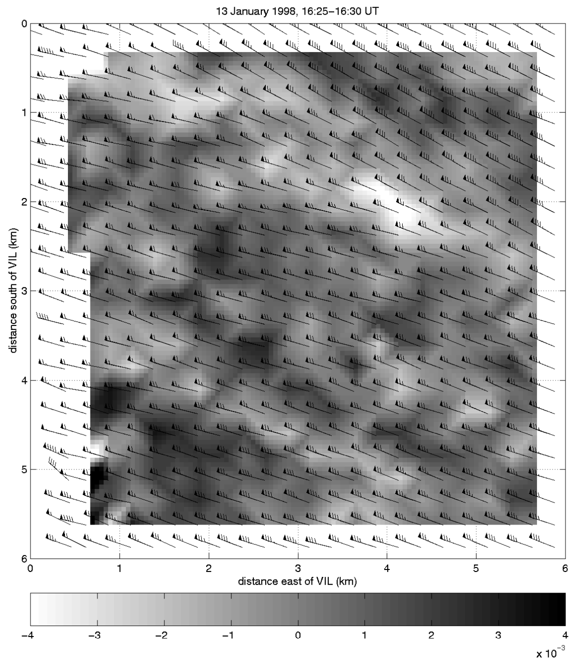

FIG. 2. Divergence of the wind field shown in fig. 1. The gray-scale ranges from ± 4x10$^{-3}$ s$^{-1}$.

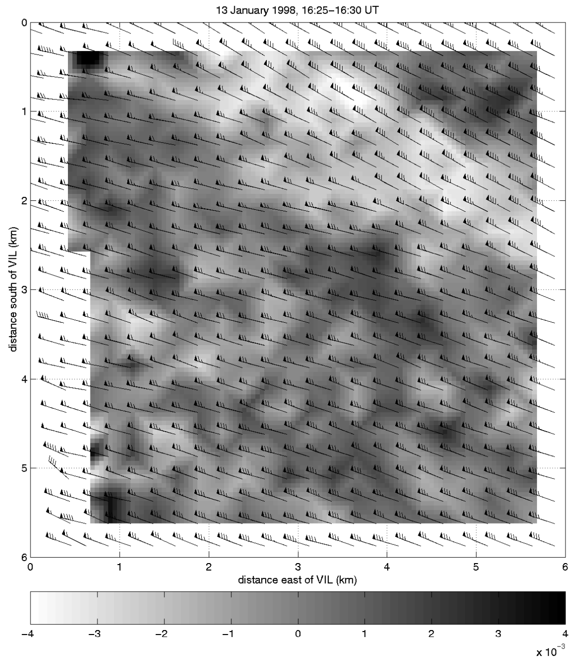

FIG. 3. Vorticity of the wind field shown in fig. 1. The gray-scale ranges from ± 4x10$^{-3}$ s$^{-1}$.

To obtain the average wind speed and direction as a function of offshore distance, we average the lidar measured wind vectors in rows that are parallel with the shore. Fig. 4 shows this result for January 10 when the flow was from the WSW. The increase in speed and change of direction is due to a reduction in surface-friction and increase in pressure-gradient.

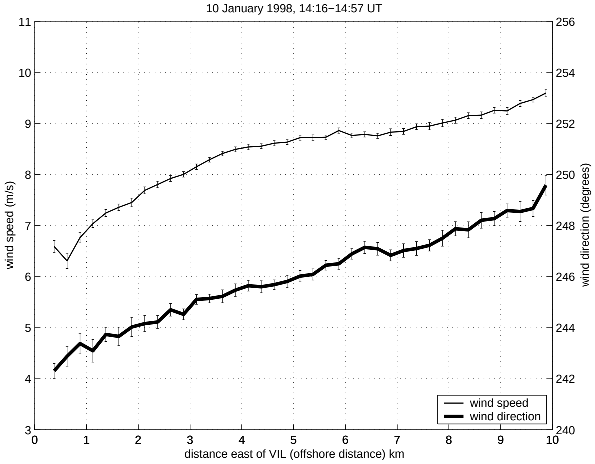

FIG. 4. Average wind speed and direction as a function of offshore direction as measured from VIL-PPI scans on 10 January 1998 from 14:16 to 14:57 CST.

The pressure gradient is caused by heating of the air over the water. However, some of the apparent speed increase and direction change may be due to the lidar scan plane sampling different altitudes. The surface of the earth lowers 15-m from a horizontal line for every 10-km distance.

## 3. Preliminary eddy-structure

To obtain the eddy-orientation with respect to the wind direction, two-dimensional covariance functions are computed from the range-corrected PPI data as a function of offshore distance according to:

$$R(x, \Delta x, \Delta y) = \frac{\sum S(x,y)S(x+\Delta x, y+\Delta y)}{\sigma_{S_1}\sigma_{S_2} n}$$

where x is the east-west direction and y is the north-south direction. $\Delta x$ and $\Delta y$ are lags in 15 m increments here. $\sigma_{S_1}$ and $\sigma_{S_2}$ are the standard deviations of the shifted and unshifted arrays. $n$ is the number of points in the arrays.

Fig. 5 is an example of just one two-dimensional covariance function from 10 January 1998 when the wind was from the WSW. 41-minutes of PPI data from a north-south band 4050-4950 m offshore was used in the calculation. The covariance function is normailzed so that it equals one at the origin. The maximum runs along the mean wind direction which is indicated with a white line. This shows that the eddies are stretched in the direction of the mean wind.

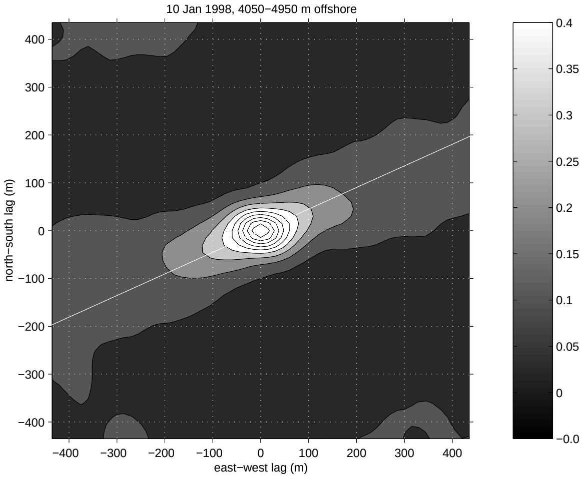

FIG. 5. Two-dimensional covariance function of the aerosol backscatter from 4-5 km offshore on 10 January 1998. The wind direction was from 245° at this range and is indicated by the white line.

## 4. Preliminary Model Results

Although our model does contain a passive tracer, we show the relative humidity (RH) fields here for comparison with the lidar aerosol backscatter data because particle size and therefore scattering are functions of RH. In the future we will combine the tracer and RH fields using known functions that relate scattering to RH to simulate lidar backscattering.

Until recently, our attempts to simulate inhomogeneous turbulent flow were achieved by using open boundary conditions on the east and west walls of the domain. We found that this caused artifical pressure gradients in the domain and so we now use periodic in the east-west. We use broad restoring zones in the ends of the domain to gently return the flow to the initial condition before it passes out the downwind wall.

In fig. 6 the lidar RHI scan shows that a 400-m deep mixed-layer is advecting offshore (top-panel). This tells us that we need more model domain over land to develop a deeper mixed layer. We intend to increase domain size in future simulations.

In fig. 7 we see interesting patterns in the steamfog that occurs near the surface. We believe the cellular appearance of the data are caused by the large-eddies coming into contact with the surface whereby they sweep up heat, moisture and particulates, and confine them to narrow walls of rising motion which make up the cells.

All the VIL data from Lake-ICE and LES-output are available as MPEG-movies and gif-files and can be downloaded from our website at http://lidar.ssec.wisc.edu.

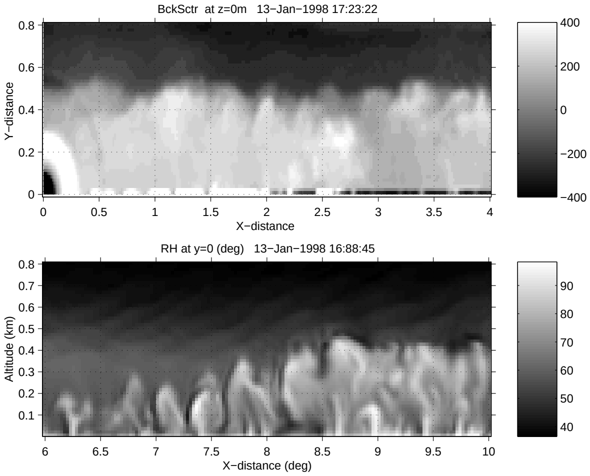

FIG. 6. One RHI scan of VIL data (top) and a vertical slice through relative humidity field of the LES domain (bottom) for comparison.

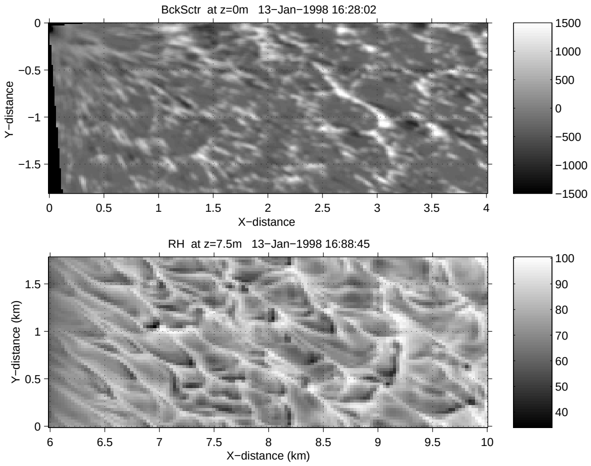

FIG. 7. One PPI scan of VIL data (top) and a horizontal slice through model domain (bottom) for comparison.

## References

1. Schols, J. L., and E. W. Eloranta, 1992: The calculation of area-averaged vertical profiles of the horizontal wind velocity from volume imaging lidar data,*J. of Geophys. Res.*, **97**, 18395-18407.

2. Pirronen, A., K. and E. W. Eloranta, 1995: Accuracy analysis of wind profiles calculated from volume imaging lidar data, *J. of Geophys. Res.*, **100**, 25559-25567.

## Acknowledgments

This work was made possible by NSF grant number ATM9707165 and ARO grant number ARO DAAH-04-94-G-0195.